RAA 2016 Vol. **16** No. **3**, 51 (10pp) doi: 10.1088/1674–4527/16/3/051
http://www.raa-journal.org *http://iopscience.iop.org/raa*

***R**esearch in*
***A**stronomy and*
***A**strophysics*

Chandra Studies of the X-ray gas properties of fossil systems

Zhen-Zhen Qin[1]

School of Science, Southwest University of Science and Technology, Mianyang 621010, China;
qin_zhenzhen@hotmail.com

Received 2015 July 17; accepted 2015 September 11

Abstract We study ten galaxy groups and clusters suggested in the literature to be "fossil systems (FSs)" based on *Chandra* observations. According to the $M_{500}-T$ and $L_{\rm X}-T$ relations, the gas properties of FSs are not physically distinct from ordinary galaxy groups or clusters. We also first study the $f_{\rm gas,\,2500}-T$ relation and find that the FSs exhibit the same trend as ordinary systems. The gas densities of FSs within $0.1r_{200}$ are $\sim 10^{-3}$ cm^{-3}, which is the same order of magnitude as galaxy clusters. The entropies within $0.1r_{200}$ ($S_{0.1r_{200}}$) of FSs are systematically lower than those in ordinary galaxy groups, which is consistent with previous reports, but we find their $S_{0.1r_{200}}-T$ relation is more similar to galaxy clusters. The derived mass profiles of FSs are consistent with the Navarro, Frenk and White model in $(0.1-1)r_{200}$, and the relation between scale radius $r_{\rm s}$ and characteristic mass density $\delta_{\rm c}$ indicates self-similarity of dark matter halos of FSs. The ranges of $r_{\rm s}$ and $\delta_{\rm c}$ for FSs are also close to those of galaxy clusters. Therefore, FSs share more common characteristics with galaxy clusters. The special birth place of the FS makes it a distinct type of galaxy system.

Key words: galaxies: cluster: general — galaxies: evolution — galaxies: halos — intergalactic medium — X-ray: galaxies: clusters

1 INTRODUCTION

Jones et al. (2003) defined a fossil group in observational terms as a spatially extended X-ray source with an X-ray luminosity from hot gas with $L_{\rm X,bol}\geq 10^{42}$ erg s^{-1}, and a bound system of galaxies with $\delta m_{12}\geq 2.0$ mag, where δm_{12} is the absolute total magnitude gap in R band between the brightest and second-brightest galaxies in the system within half of the (projected) virial radius. Thus, it is a galaxy group dominated by one central luminous giant elliptical galaxy with few, or no, L^* galaxies inside the radius due to orbital decay by dynamical friction. There also exist some fossil clusters like RX J1416.4+4018 and AWM 4. We call such a galaxy group or cluster a fossil system (FS) throughout this paper. High values of δm_{12} are extremely rare in ordinary galaxy groups or clusters (Beers et al. 1995), which is why an FS is believed to be a distinct type of galaxy system.

However, the origin and evolution process of an FS are still not well understood and have many discrepancies. There are mainly three scenarios on the origin of an FS that were proposed in previous works: (1) the FS may be the end result of galaxy merging within a normal group (Ponman et al. 1994; Jones et al. 2000); (2) the birth place of the FS may be isolated and deficient in L^* galaxies (Mulchaey & Zabludoff 1999); (3) the FS is a transient yet common phase in the evolution of groups or clusters, ending with the infall of fresh galaxies from the surroundings (von Benda-Beckmann et al. 2008). The discrepancies of its evolution process mainly focus on two points: whether the FS is the descendant of the compact group (Yoshioka et al. 2004; Mendes de Oliveira & Carrasco 2007), and the relation between the FS and the galaxy cluster (Khosroshahi et al. 2006; Méndez-Abreu et al. 2012). Simulations indicate FSs assemble a large fraction of their mass at high redshifts, which means FSs are formed earlier than ordinary systems (Dariush et al. 2007; Dariush et al. 2010). Much effort has been devoted to understanding the origin and evolution of FSs via their optical properties, such as the photometric luminosity function, the stellar population ages and the isophotal shapes of the brightest galaxies in FSs (Adami et al. 2012; Aguerri et al. 2011; Khosroshahi et al. 2006). There are also some systematic X-ray studies on hot gas properties of FSs (Khosroshahi et al. 2007; Miller et al. 2012).

In this paper, we analyze the *Chandra* archive data of ten FSs to determine their X-ray characteristics, including temperatures, masses, luminosities, gas fractions and entropies. The scaling relations between them are used to infer the gas accretion history and heating process in FSs. We also study dark matter halo structures of FSs.

We describe the sample selection criteria and data analysis in Section 2 and Section 3, respectively. Sections 4, 5 and 6 present results of our sample study and discuss the physical implications. We summarize our work in Section 7. We assume $H_0=70$ km s^{-1} Mpc^{-1}, a

flat universe for which $\Omega_{\rm m} = 0.3$ and $\Omega_\Lambda = 0.7$, and adopt the solar abundance standards of Grevesse & Sauval (1998), where the iron abundance relative to hydrogen is 3.16×10^{-5} in number. Unless stated otherwise, all quoted errors are derived at the 68% confidence level.

2 SAMPLE AND DATA PREPARATION

We construct our sample of ten FSs (including eight fossil groups and two fossil clusters) with $z \leq 0.4$, which are chosen from confirmed FSs in previous works. Six of them are observed by the S3 CCD of the *Chandra* advanced CCD imaging spectrometer (ACIS) instrument, and the remaining four are observed by the ACIS I CCDs. We list basic properties of the sample in Table 1, which are arranged according to object names (col. [1]), right ascension and declination coordinates (J2000) of the FS optical centroids (col.[2] and col.[3] respectively), redshifts (col.[4]), detectors (col.[5]), exposure times (col.[6]), *Chandra* Observational ID (col.[7]) and reference (col.[8]).

All the X-ray data analyzed in this work are acquired with the temperature of the ACIS S/I CCDs set to be -120 °C. Using the CIAO software (version 3.4), we keep events with ASCA grades 0, 2, 3, 4 and 6, remove all the bad pixels and columns, columns adjacent to bad columns and node boundaries, and then exclude the gain, charge transfer inefficiency and astrometry corrections. In order to identify possible strong background flares, light curves are extracted from regions sufficiently far away. Time intervals during the count rate exceeding the average quiescent value by 20 percent are excluded.

3 DATA ANALYSIS

3.1 Spectral Analysis

We utilize the *Chandra* blank-sky template for the ACIS CCDs as the background. The template is tailored to match the actual pointing. The background spectrum is extracted and processed identically to the source spectrum. Then we rescale the background spectrum by normalizing its high energy end to the corresponding observed spectrum. The corresponding spectral redistribution matrix file (RMFS) and auxiliary response files (ARFS) are created by using the CIAO tools $mkwarf$ and $mkacisrmf$, respectively. All spectra are rebinned to insure at least 20 raw counts per spectral bin to allow χ^2 statistics to be applied. Since the contribution of the hard spectral component is expected to be rather weak, and also to minimize the effects of the instrumental background at higher energies as well as the calibration uncertainties at lower energies, the fittings were restricted to $0.7 - 7.0$ keV.

Due to the sufficient count numbers, we can extract deprojected temperature profiles of five FSs: AWM 4, ESO 306017, NGC 1550, NGC 6482 and SDSS J1720+2637, where we use the XSPEC model $projct$ to evaluate the influence of the outer spherical shells on the inner ones. We model the hot gas with an absorbed APEC component in every annulus, with an additional power-law component subject to the same absorption to constrain the contribution from unresolved Low Mass X-ray Binaries. The absorption ($N_{\rm H}$) of each FS is fixed at the Galactic value (Dickey & Lockman 1990) throughout. The spectra are fitted with XSPEC v.12.3.1x. The best-fit deprojected gas temperature profiles of these five FSs are shown in Figure 1. To describe the obtained deprojected best-fit temperature profiles in a smooth form, we adopt the analytic model based on the formulation introduced in Allen et al. (2001),

$$T(r) = T_0 + T_1 \frac{(r/r_{\rm tc})^\eta}{(1 + (r/r_{\rm tc})^\eta)^\eta}\,, \qquad (1)$$

where T_0, T_1 and $r_{\rm tc}$ are fitting parameters with fixed $\eta = 2$. We note that our temperature model differs from that of Allen et al. (2001) in two aspects: (i) it models the radius and temperature in physical units rather than normalized to their value at R_{2500} like in the model published by Allen et al. (2001); (ii) our model has an extra "η" to better describe the temperature drop at outer regions of galaxy groups and clusters. The best-fit T_0, T_1 and $r_{\rm tc}$ are listed in Table 2, and the smoothed deprojected temperature profiles are also shown in Figure 1. One can see AWM 4 shows a nearly isothermal temperature profile, which was reported by O'Sullivan et al. (2005). NGC 6482 shows a hot core in its temperature profile, which was ascribed to possible AGN activity in the group center (Khosroshahi et al. 2004). The other three FSs show central temperature decreases, which indicate residing cool cores and have no ongoing major mergers.

Due to the limited counts, it is insufficient to extract the deprojected temperature profiles of the other five FSs. Therefore, we obtain the global temperature of these five FSs by extracting global ACIS spectra from a circular region with the center on the peak of the emission corresponding to the maximum measured extent of the X-ray emission. The gas is also modeled with an APEC component plus a power-law component, both subjected to a common absorption as above. Best-fit global temperatures $T_{\rm g}$ of these five members are also listed in Table 2.

3.2 Surface Brightness Profile and Gas Density

The *Chandra* images of members in the FS sample all exhibit relaxed, regular and symmetric morphology. For every FS, the peak of the X-ray emission is consistent with the centroid of the cD galaxy within $1''$. We exclude all the visual point sources of FSs, which could be detected at a 3σ confidence level by the CIAO tool *celldetect*. The X-ray radial surface brightness profiles (SBPs) are extracted from a series of annular regions centered on the X-ray emission peak and extending near the boundary of CCD detections. The energy band of SBPs is restricted to the ACIS images in the $0.7 - 7.0$ keV band with exposure being corrected. Such extracted SBPs are shown in Figure 2.

Assuming spherical symmetry, we deprojected the SBP to generate the 3-dimensional electron number density profile $n_{\rm e}(r)$ of the intergalactic medium with the

Table 1 FSs in Our Sample

Object name	RA[b] (h m s)	Dec[b] (° ′ ″)	Redshift	Detector	Exp (ks)	ObsID	Reference[c]
AWM 4[a]	16 04 57.0	+23 55 14	0.032	ACIS-S	75	9423	[1]
ESO 306017	05 40 06.7	–40 50 11	0.036	ACIS-I	14	3188	[2]
NGC 1132	02 52 51.8	–01 16 29	0.023	ACIS-S	40	3576	[3]
NGC 1550	04 19 37.9	+02 24 36	0.012	ACIS-I	10	3186	[4]
NGC 6482	17 51 48.8	+23 04 19	0.013	ACIS-S	20	3218	[5]
NGC 741	01 56 21.0	+05 37 44	0.019	ACIS-S	31	2223	[6]
RX J1340.6+4018	13 40 09.0	+40 17 43	0.171	ACIS-S	48	3223	[1]
RX J1416.4+2315[a]	14 16 26.0	+23 15 23	0.138	ACIS-S	14	2024	[1]
SDSS J0150–1005	01 50 21.3	–10 05 31	0.364	ACIS-I	27	11711	[7]
SDSS J1720+2637	17 20 10.0	+26 37 32	0.159	ACIS-I	26	4631	[7]

Notes: [a] AWM 4 is a poor galaxy cluster, and RX J1416.4+2315 was identified as a fossil cluster (Cypriano et al. 2006). [b] Positions of FS optical centroids (J2000). [c] References include [1] Zibetti et al. (2009), [2] Sun et al. (2004), [3] Yoshioka et al. (2004), [4] Sato et al. (2010), [5] Khosroshahi et al. (2004), [6] Rasmussen & Ponman (2007), and [7] Santos et al. (2007).

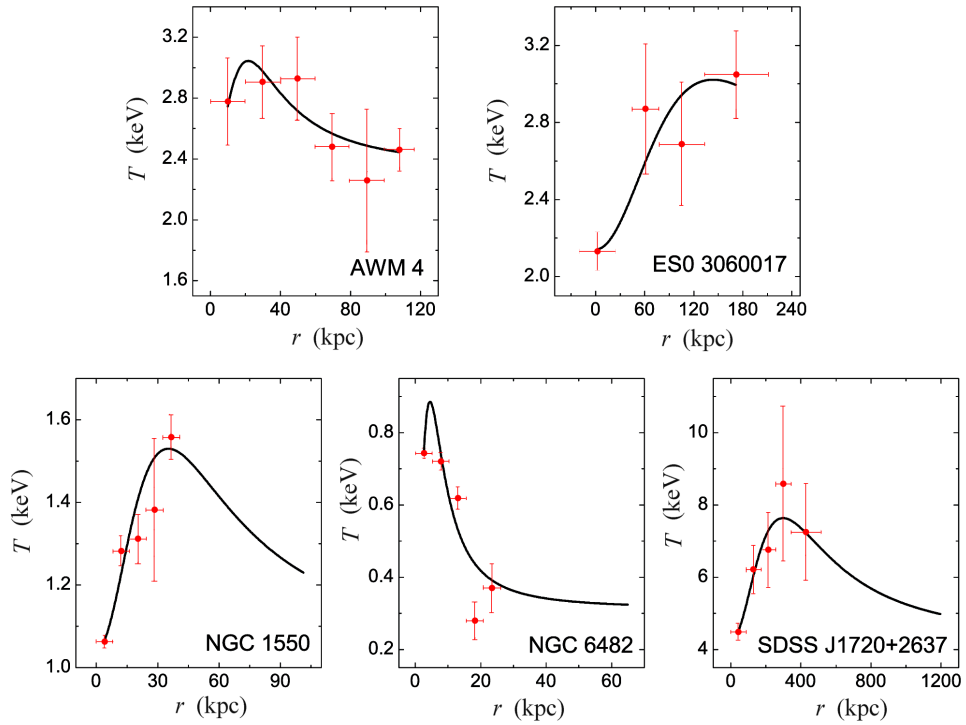

Fig. 1 The deprojected temperature profiles of five FSs with sufficient counts. Solid lines are the best-fit deprojected temperature profiles.

standard "onion-skin" method (Kriss et al. 1983). During the deprojection, we assume five FSs are isothermal at the best-fit global temperatures $T_{\rm g}$ listed in Table 2, including NGC 1131, NGC 741, RX J1340.6+4018, RX J1416.4+2315 and SDSS J0150−1005. For the other five FSs, temperature profiles shown in Figure 1 are applied. We believe that uncertainties from our choice of the gas temperature would not significantly affect resultant electron density profiles, because Kriss et al. (1983) have pointed out that the deduced density profile is actually very insensitive to temperature.

With the single-β model, we fit the $n_{\rm e}(r)$ of seven FSs as

$$n_{\rm e}(r) \;=\; n_0[1+(r/r_{\rm c})^2]^{-1.5\beta} + n_{\rm bkg}\,, \qquad (2)$$

where r is the 3-dimensional radius, n_0 corresponds to the normalization, $r_{\rm c}$ is the core radius, β is the slope and $n_{\rm bkg}$ is the background. The single-β model fails when applied to the other three FSs, because these FSs have central emission that is not able to be described by the single-β model, which is more appropriate for describing the SBPs of outer regions. To overcome this limitation, we use a double-β model to describe the spatial distribution of $n_{\rm e}(r)$ in the

Table 2 Gas Properties of FSs

Object name	$T_{\rm g}^{a}$ (keV)	T_0^{b} (keV)	T_1^{b} (keV)	$r_{\rm tc}^{b}$ (kpc)	r_{200} (Mpc)	$T_{0.1{\rm r}_{200}}$ (keV)	$n_{\rm e,\,0.1r_{200}}$ (10^{-3} cm^{-3})
AWM 4	$--$	2.34 ± 0.17	2.81 ± 1.37	21.62 ± 7.21	0.90 ± 0.05	2.72 ± 0.05	2.83 ± 0.32
ESO 306017	$--$	2.14 ± 0.09	3.53 ± 0.87	143.56 ± 52.91	1.07 ± 0.03	2.97 ± 0.19	2.65 ± 0.12
NGC 1132	1.06 ± 0.01	$--$	$--$	$--$	0.62 ± 0.008	1.04 ± 0.01	1.40 ± 0.38
NGC 1550	$--$	1.04 ± 0.02	1.95 ± 0.21	35.22 ± 4.76	0.42 ± 0.02	1.31 ± 0.009	6.78 ± 0.72
NGC 6482	$--$	0.31 ± 0.04	2.29 ± 0.28	4.5 ± 0.14	0.53 ± 0.004	0.65 ± 0.01	1.08 ± 0.13
NGC 741	0.99 ± 0.02	$--$	$--$	$--$	0.64 ± 0.006	1.05 ± 0.02	1.18 ± 0.14
RX J1340.6+4018	1.23 ± 0.06	$--$	$--$	$--$	0.64 ± 0.02	1.15 ± 0.14	3.71 ± 0.56
RX J1416.4+2315	4.23 ± 0.43	$--$	$--$	$--$	1.21 ± 0.06	4.00 ± 0.62	2.77 ± 0.14
SDSS J0150–1005	5.61 ± 0.52	$--$	$--$	$--$	1.55 ± 0.11	5.28 ± 0.46	4.63 ± 0.75
SDSS J1720+2637	$--$	4.23 ± 0.32	13.62 ± 3.65	298.46 ± 85.94	1.51 ± 0.08	4.47 ± 0.49	9.63 ± 0.24

Notes: [a] Global temperatures of five FSs with insufficient counts, which are extracted from a circular region with the center on the peak of emission corresponding to the maximum measured extent of the X-ray emission. [b] Best-fit model parameters for deprojected temperature profiles of five FSs with sufficient counts. We plot the best-fit deprojected temperature profiles as solid lines in Fig. 1.

Table 3 Best-fit Density Model Parameters

Object name	$\beta(\beta_1)$	$n_0(n_1)^{a}$ (10^{-2} cm^{-3})	$r_{\rm c}(r_{\rm c1})^{a}$ (kpc)	β_2	n_2 (10^{-2} cm^{-3})	$r_{\rm c2}$ (kpc)	$\chi^2/{\rm dof}^{b}$
AWM 4	0.56 ± 0.01	4.00 ± 0.20	1.34 ± 0.19	0.48 ± 0.01	0.61 ± 0.04	31.28 ± 1.35	113.14/104
ESO 306017	0.56 ± 0.01	7.24 ± 0.18	3.18 ± 0.14	0.46 ± 0.01	0.38 ± 0.01	56.06 ± 116	117.31/114
NGC 1132	0.40 ± 0.01	14.82 ± 2.28	0.70 ± 0.12	$--$	$--$	$--$	94.99/56
NGC 1550	0.35 ± 0.01	9.35 ± 0.83	2.16 ± 0.03	$--$	$--$	$--$	119.47/114
NGC 6482	0.50 ± 0.01	14.71 ± 0.90	1.13 ± 0.06	$--$	$--$	$--$	78.43/68
NGC 741	0.46 ± 0.01	22.32 ± 1.41	0.83 ± 0.05	$--$	$--$	$--$	118.66/76
RX J1340.6+4018	0.42 ± 0.01	1.44 ± 0.14	13.80 ± 1.40	$--$	$--$	$--$	68.97/66
RX J1416.4+2315	0.42 ± 0.01	0.50 ± 0.02	57.92 ± 1.40	$--$	$--$	$--$	77.17/59
SDSS J0150−1005	0.65 ± 0.02	5.40 ± 0.41	15.48 ± 1.59	0.64 ± 0.01	0.52 ± 0.01	107.43 ± 14.75	97.42/94
SDSS J1720+2637	0.54 ± 0.01	4.88 ± 0.07	36.11 ± 0.54	$--$	$--$	$--$	169.36/96

Notes: [a] For the single-β fitted FS these two columns represent n_0 and $r_{\rm c}$, respectively, and for the double-β fitted FS these two columns represent n_1 and $r_{\rm c1}$, respectively. [b] Reduced Chi-square value for the best fit of single-β or double-β model.

other three FSs

$$n_{\rm e}(r) = n_1[1+(r/r_{\rm c1})^2]^{-1.5\beta_1} + n_2[1+(r/r_{\rm c2})^2]^{-1.5\beta_2} + n_{\rm bkg}\,. \quad (3)$$

We list the best-fit parameters of $n_{\rm e}(r)$ in Table 3. The best-fit electron number density profiles and SBPs are presented in Figures 2 and 3, respectively.

4 HOT GAS PROPERTIES

In this section, we present hot gas properties of FSs, e.g. the relations between gravitational mass, X-ray luminosity (L_x), gas fraction ($f_{\rm gas}$), entropy and system temperature (T). The spectral temperatures within the $0.1r_{200}$ region are used as the system temperature T. First of all, we determine the radii r_{200}, r_{500} and r_{2500}, within which the respective average mass density is 200, 500 and 2500 times the critical density of the universe at corresponding redshift (we will introduce calculation of mass in Section 4.1). Table 2 lists all the values of virial radius r_{200} of our sample in detail. The total mass within r_{500} is denoted as M_{500}, which is used to examine the $M_{500}-T$ relation of FSs. The bolometric $L_{\rm X}$ of the FS is taken to be within r_{200}. Then, we derive the gas fraction $f_{\rm gas}$, which is the mass ratio of the hot gas component to the total mass. $f_{\rm gas,\,2500}$ means the gas fraction at r_{2500}. Finally, we calculate entropies within $0.1r_{200}$ of FSs.

4.1 $M_{500}-T$ and $L_{\rm X}-T$ Relations

In a spherically symmetric system with hydrostatic equilibrium, $M_{\rm tot}(<r)$, the total mass within a given radius, r, is given by

$$M_{\rm tot}(<r) = \frac{-r^2 k_{\rm B}}{G\mu m_{\rm p} n_{\rm e}(r)} \frac{d[n_{\rm e}(r)T(r)]}{dr}\,, \quad (4)$$

where G is the universal gravitational constant, $k_{\rm B}$ is the Boltzmann constant, $\mu = 0.62$ is the mean molecular weight per hydrogen atom, $m_{\rm p}$ is the proton mass, $n_{\rm e}(r)$ is the electron number profile, and $T(r)$ is the temperature profile. In the $M_{\rm tot}(<r)$ calculation, all the gas temperature profiles, $T(r)$, are directly taken from Table 2. $n_{\rm e}(r)$ is obtained from the best-fitting of the X-ray surface brightness profile described in Table 3. In detail, we use $T(r)$ as the spectral modeling of the five FSs with sufficient counts, and assume a constant $T(r)$ for the remaining five FSs, where one can only calculate the global temperatures $T_{\rm g}$. With Equation (4) and 1000 Monte Carlo simulations, M_{500} and its error are readily derived.

Values for the luminosity $L_{\rm X}$ of the FSs within r_{200} are given by $L_{\rm X} = \iiint \Lambda n_{\rm e} n_{\rm H} dV$, where Λ is the cooling function and $n_{\rm H}$ is the proton number density. We calculate the integral of the electron number density profile to derive the bolometric $L_{\rm X}$. The error in $L_{\rm X}$ is obtained from the Poisson error in the X-ray count rate.

Figure 4 shows the $M_{500}-T$ relation of FSs compared with galaxy groups and clusters from Sun et al. (2009) and

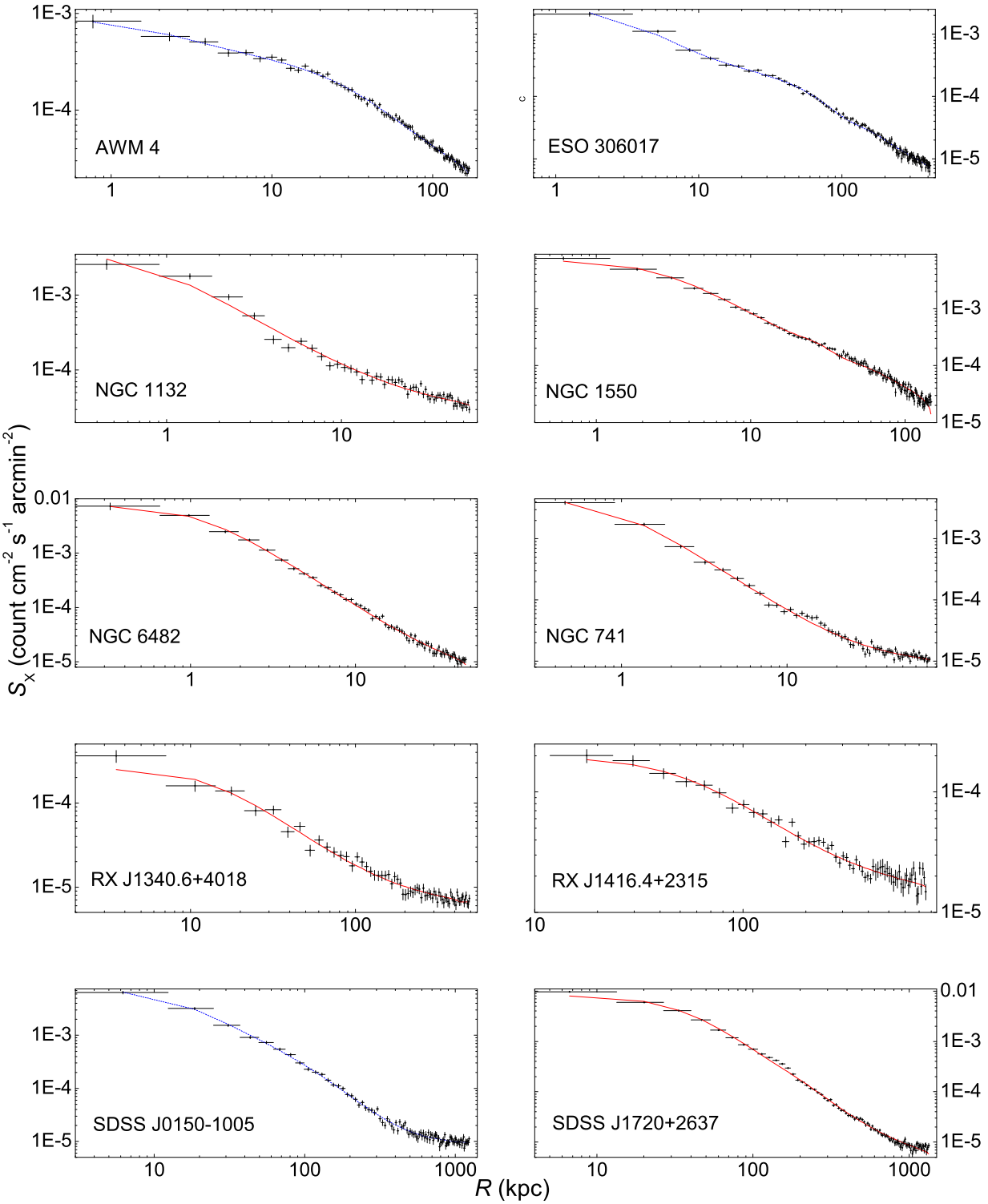

Fig. 2 Exposure-corrected SBPs extracted from a series of annular regions centered on the X-ray emission peak of the FSs. R is the projected distance. The solid lines and dotted lines correspond to the best-fit single-β and double-β SBPs, respectively.

Arnaud et al. (2005), respectively. The slope of the best linear fit to all the data is 1.67 ± 0.04, which is consistent with the value of previous work, 1.78 ± 0.09, within errors (Finoguenov et al. 2001). Figure 5 presents the $L_{\rm X} - T$ relation of FSs compared with non-fossil galaxy groups and clusters from the sample of Helsdon & Ponman (2000) and Wu et al. (1999), respectively. The $M_{500} - T$ and $L_{\rm X} - T$ relations of FSs exhibit no obvious deviation from non-fossil galaxy groups and clusters.

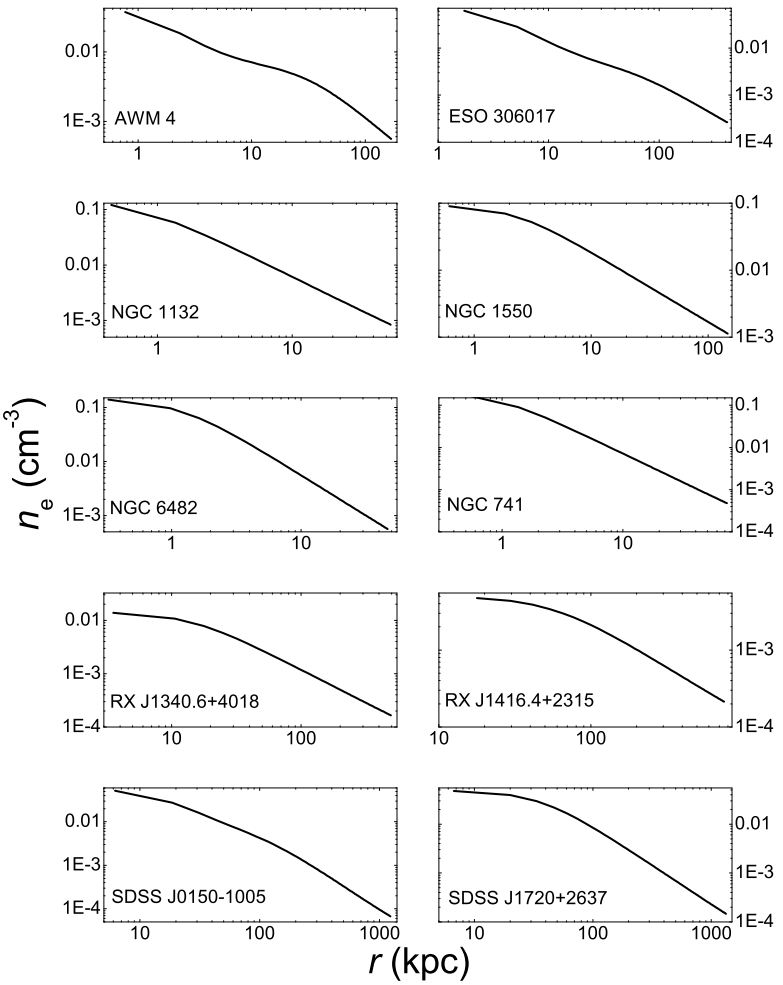

Fig. 3 Gas density profiles obtained from the deprojection of the SBPs.

4.2 Gas Fraction of FSs

With $n_{\rm e}(r)$ from Section 3.2, we calculate the $f_{\rm gas}$ for FSs at r_{200}, r_{500} and r_{2500}. The gas fractions increase with radius in FSs, which is consistent with ordinary systems (Gastaldello et al. 2007). Typically, we present the $f_{\rm gas,\,2500}-T$ relation in Figure 6 compared with 43 galaxy groups (Sun et al. 2009) and 14 galaxy clusters (Vikhlinin et al. 2006, 2009). In our sample, seven higher temperature FSs show a nearly constant gas fraction with a mean value of $f_{\rm gas,\,2500}$, 0.073 ± 0.007, while the other three lower temperature FSs exhibit decreased $f_{\rm gas,\,2500}$. The $f_{\rm gas,\,2500} - T$ relation in FSs is consistent with previous works, which have reported that $f_{\rm gas,\,2500}$ remains quite constant over higher temperature galaxy systems, yet detected a decrease in the low mass, low temperature end (Gastaldello et al. 2007; Dai et al. 2010).

4.3 Entropy Within $0.1r_{200}$

The gas entropy is defined as

$$S = T/n_{\rm e}^{2/3}\,, \tag{5}$$

where $n_{\rm e}$ is the electron number density. We calculate the gas entropy at $0.1r_{200}$, $S_{0.1{\rm r}_{200}}$. Because $0.1r_{200}$ is very close to the center, we can avoid the shock-generated entropy and thus enhance the sensitivity to any additional entropy. Figure 7 shows the entropies of FSs compared with Ponman et al. (2003). The entropies of FSs are systematically lower than those of the non-fossil galaxy groups, and the $S_{0.1r_{200}}-T$ plots of FSs are roughly around the dashed line in Figure 7, which has a self-similar slope of 1, normalized to the mean entropy of the hottest eight clusters in Ponman et al. (2003). We also list $n_{\rm e}$ within $0.1r_{200}$ regions of FSs in Table 2, which are $\sim 10^{-3}$ cm^{-3}, the same order of magnitude as galaxy clusters, but higher than those of galaxy groups.

5 DARK MATTER HALO STRUCTURES

As suggested by high-resolution N-body simulations, the Navarro et al. (1996) (hereafter NFW) model is used to describe the mass profile of all the dark matter halos

$$\rho(r) = \frac{\rho_0 \delta_{\rm c}}{(r/r_{\rm s})(1+r/r_{\rm s})^2}\,, \tag{6}$$

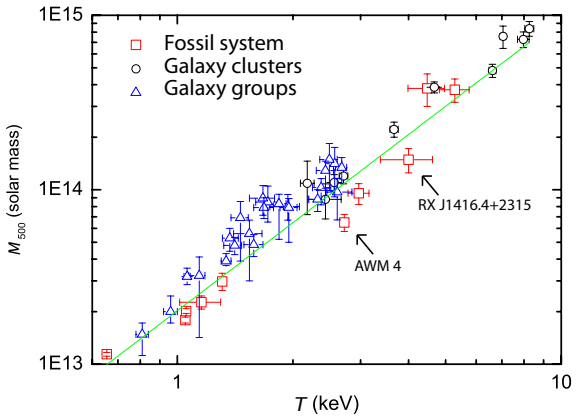

Fig. 4 $M_{500} - T$ relation for FSs compared with ordinary galaxy groups and clusters. The red squares represent FSs, black circles correspond to galaxy clusters derived from Arnaud et al. (2005), and blue triangles correspond to galaxy groups derived from Sun et al. (2009). Two fossil clusters in the sample, AWM 4 and RX J1416.4+2315, are marked. The green solid line is the best linear fit to all the data with a slope of 1.67 ± 0.04.

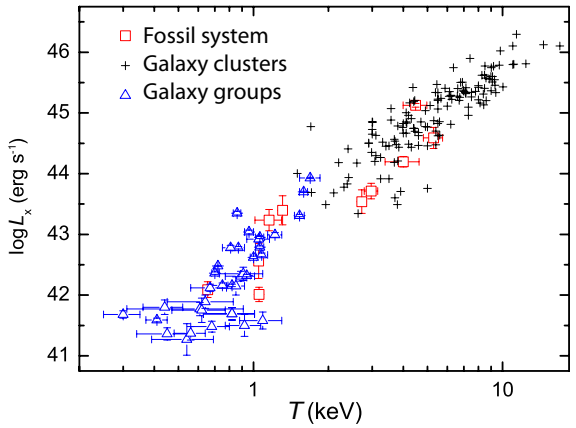

Fig. 5 $L_{\rm X} - T$ relation of FSs compared with non-fossil systems. Red squares represent FSs, black crosses correspond to galaxy clusters derived from Wu et al. (1999), and blue triangles correspond to galaxy groups derived from Helsdon (2000). The sample of FSs falls on the $L_{\rm X} - T$ relation exhibited by non-fossil systems.

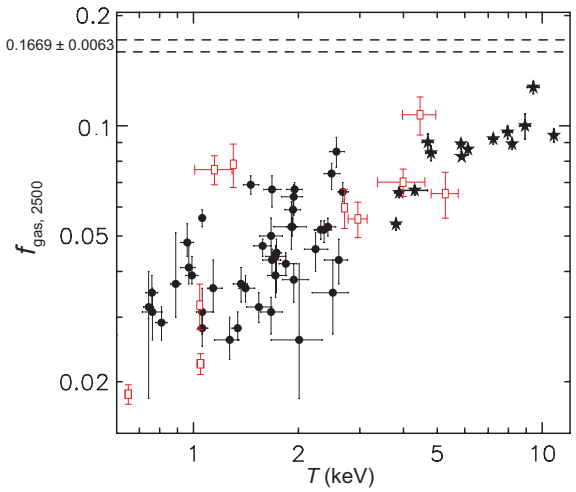

Fig. 6 $f_{\rm gas,\ 2500}$ of the FSs sample compared with ordinary systems. Red squares represent the FSs, filled circles correspond to 43 galaxy groups from Sun et al. (2009), and filled stars correspond to 14 galaxy clusters from Vikhlinin et al. (2006, 2009). Two dashed lines enclose the 1σ region of the universal baryon fraction derived from the *WMAP* 5-year data combined with the data from type Ia supernovae and baryon acoustic oscillations (0.1669 ± 0.0063, Komatsu et al. 2009).

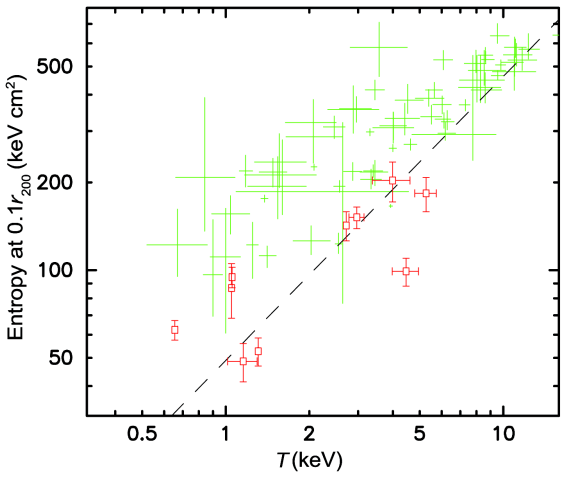

Fig. 7 Gas entropy at $0.1r_{200}$ as a function of system temperature for FSs (*red squares*) compared with non-fossil galaxy groups and clusters (*green crosses*) from Ponman et al. (2003). The dashed line is the extrapolation of self-similarity normalized to the mean entropy of the hottest eight clusters in Ponman et al. (2003).

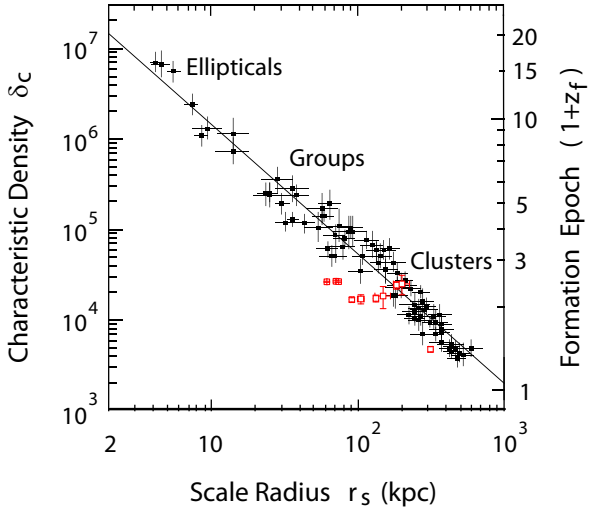

Fig. 8 The $\delta_{\rm c} - r_{\rm s}$ relation. Red squares show FSs and black filled squares represent ellipticals, groups and clusters from Sato et al. (2000). Dark matter halos of FSs assembled approximately at the epoch of $1 + z_{\rm f} \simeq 2 - 3$.

where ρ is the mass density, $r_{\rm s}$ is the scale radius, ρ_0 is the critical density of the universe, and $\delta_{\rm c}$ is the characteristic density. With the NFW model, we can obtain the following integrated profile of a spherical mass distribution,

$$M_{\rm tot}(< r) = 4\pi\delta_{\rm c}\rho_0 r_{\rm s}^3\Big[\ln\Big(1+\frac{r}{r_{\rm s}}\Big) - \frac{r}{r+r_s}\Big]. \quad (7)$$

We fit the NFW mass profile, Equation (7), to our X-ray derived total mass profile of FSs in $(0.1-1)r_{200}$ to determine $r_{\rm s}$ and $\delta_{\rm c}$.

Figure 8 shows the relation between $r_{\rm s}$ and $\delta_{\rm c}$ of FSs. The FSs show a similar correlation between $\delta_{\rm c}$ and $r_{\rm S}$ to that in Sato et al. (2000), which indicates the self-similarity of dark matter halos. According to the range of $r_{\rm s}$ and $\delta_{\rm c}$, the sizes of dark matter halos of FSs are more similar to those of galaxy clusters.

Since the density profile of a dark halo is only rearranged by a major merger, it indicates when the last merger took place: each $\delta_{\rm c}$ in the NFW model corresponds to a formation epoch of the associated dark matter halo. Therefore, dark matter halos of FSs were assembled at approximately $1 + z_{\rm f} \simeq 2 - 3$ as shown in Figure 8.

6 DISCUSSION

In Section 4 and Section 5, we present hot gas properties and dark matter halo structures of FSs. The gas properties of FSs are not physically distinct from those of ordinary systems, but their special birth places make FSs a distinct type of galaxy system. In detail, we discuss this result as follows.

First of all, according to Figures 4–5, the FSs have similar $M_{500} - T$ and $L_{\rm x} - T$ relations to those of normal groups and clusters, which means the gas properties of FSs are not physically distinct from normal objects. In the standard picture of hierarchical structure formation, groups comprising a handful of galaxies merge through gravity to form large clusters of hundreds of galaxies. The $M_{500} - T$ and $L_{\rm X} - T$ relations also indicate that FSs follow the standard picture, and belong to a common class of virialized systems in the hierarchical structure forming universe. We also present the $f_{\rm gas,\ 2500} - T$ relation of FSs in Figure 6, which agrees with current observations (Gastaldello et al. 2007; Dai et al. 2010). In simulation, the gas fraction is directly related to the strength of cooling, star formation and AGN activity in the galaxy group and cluster (e.g., Kravtsov et al. 2005; Puchwein et al. 2008). Therefore, our result indicates these non-gravitational events in FSs may be as active as ordinary systems. This is supported by a study on the level of AGN activity in fossil systems (Hess et al. 2012). In summary, the gas properties of FSs are not physically distinct from those of ordinary systems.

Secondly, we examine the entropies within $0.1r_{200}$ of our sample. As shown in Figure 7, the entropies of FSs are systematically lower than those of ordinary galaxy groups or clusters. If FSs evolve from normal galaxy groups through a fast and efficient process of merging, the merger shocks during this process would generate entropy, so that the FSs have higher entropy than normal galaxy groups (Tozzi et al. 2000). This is opposite to our result. Therefore, FSs are unlikely to be formed through a fast and efficient merging of normal galaxy groups.

On the other hand, the $S_{0.1r_{200}} - T$ relation follows the self-similar extrapolation of rich-cluster entropies. In previous work, entropy excesses in the inner regions of galaxy groups and clusters are explained by the pre-heating scenario, which suggests the existence of a universal entropy floor. The entropy excess is greater in lower temperature systems (Ponman et al. 1999; Finoguenov et al. 2002). As presented in Figure 7, the entropy excess in FSs is less than that in ordinary galaxy groups, but at the same level as ordinary galaxy clusters. The gravitational collapse of galaxy clusters happened earlier than the galaxy groups, which means the entropy excess is greater in cooler systems: in hotter clusters the gravitational collapse of the system generates entropies in excess of the floor value established by preheating, but in cooler systems it is preserved during collapse, and prevents the gas from collapsing to high central densities (Ponman et al. 1999). Therefore, FSs may collapse as early as galaxy clusters, and FSs are more similar to galaxy clusters in the preheating history.

Finally, we study dark matter halo structures of FSs by fitting the mass profile with the NFW model. As shown in Figure 8, the dark matter halo structures of FSs are similar to those of ordinary objects (Sato et al. 2000). The range of FS $r_{\rm s}$ and $\delta_{\rm c}$ is closer to that of galaxy clusters, which indicates that FSs and galaxy clusters may have nearly the same size dark matter halos. According to Sato et al. (2000), dark matter halos of FSs were assembled approximately at $1 + z_{\rm f} \simeq 2 - 3$, which means the forming epoch of FSs is later than that for the galaxy groups, but at the same time as galaxy clusters. This is consistent with the simulation of Díaz-Giménez et al. (2008), who points out that the first-ranked galaxies in fossil systems merged later than their non-fossil-system counterparts.

FSs share many common characteristics with galaxy clusters. Their gravitational collapse times and dark matter halo sizes are nearly the same, and also the $n_{\rm e}$ within $0.1r_{200}$ regions of FSs are $\sim 10^{-3}$ cm^{-3}, the same order of magnitude as galaxy clusters. Why do the FSs have large magnitude gaps which are distinct from an ordinary galaxy cluster? We prefer the answer that the birth places of FSs may be isolated and deficient in L^* galaxies, so that the FSs exhibit large magnitude gaps compared with galaxy clusters. All in all, we would conclude that the special birth place of the FS makes it a distinct type of galaxy system.

7 SUMMARY

By using *Chandra* X-ray observations of a sample of ten FSs, we study their $M_{500} - T$, $L_{\rm X} - T$ and $f_{\rm gas,\ 2500} - T$ relations, and find the hot gas properties of FSs are not physically distinct from ordinary systems. By analyzing the gas densities, entropies and dark matter halos of FSs, we also find FSs share common characteristics with galaxy clusters, such as they have almost the same gas densities, gravitational collapse times and dark matter halo sizes. Therefore, we prefer the scenario that the birth place of an FS may be isolated and deficient in L^* galaxies, which makes it a distinct type of galaxy system.

Acknowledgements This work is supported by the Research Fund for the Doctoral Program of the Southwest University of Science and Technology (No. 14zx7102).

References

Adami, C., Jouvel, S., Guennou, L., et al. 2012, A&A, 540, A105
Aguerri, J. A. L., Girardi, M., Boschin, W., et al. 2011, A&A, 527, A143
Allen, S. W., Schmidt, R. W., & Fabian, A. C. 2001, MNRAS, 328, L37
Arnaud, M., Pointecouteau, E., & Pratt, G. W. 2005, A&A, 441, 893
Beers, T. C., Kriessler, J. R., Bird, C. M., & Huchra, J. P. 1995, AJ, 109, 874
Cypriano, E. S., Mendes de Oliveira, C. L., & Sodré, Jr., L. 2006, AJ, 132, 514
Dai, X., Bregman, J. N., Kochanek, C. S., & Rasia, E. 2010, ApJ, 719, 119
Dariush, A., Khosroshahi, H.G, Ponman, T. J., et al. 2007, MNRAS, 382, 433
Dariush, A. A., Raychaudhury, S., Ponman, T. J., et al. 2010, MNRAS, 405, 1873

Díaz-Giménez, E., Muriel, H., & Mendes de Oliveira, C. 2008, A&A, 490, 965
Dickey, J. M., & Lockman, F. J. 1990, ARA&A, 28, 215
Finoguenov, A., Reiprich, T. H., & Böhringer, H. 2001, A&A, 368, 749
Finoguenov, A., Jones, C., Böhringer, H., & Ponman, T. J. 2002, ApJ, 578, 74
Gastaldello, F., Buote, D. A., Humphrey, P. J., et al. 2007, ApJ, 669, 158
Grevesse, N., & Sauval, A. J. 1998, Space Sci. Rev., 85, 161
Helsdon, S. F., & Ponman, T. J. 2000, MNRAS, 319, 933
Hess, K. M., Wilcots, E. M., & Hartwick, V. L. 2012, AJ, 144, 48
Jones, L. R., Ponman, T. J., & Forbes, D. A. 2000, MNRAS, 312, 139
Jones, L. R., Ponman, T. J., Horton, A., et al. 2003, MNRAS, 343, 627
Khosroshahi, H. G., Jones, L. R., & Ponman, T. J. 2004, MNRAS, 349, 1240
Khosroshahi, H. G., Ponman, T. J., & Jones, L. R. 2006, MNRAS, 372, L68
Khosroshahi, H. G., Ponman, T. J., & Jones, L. R. 2007, MNRAS, 377, 595
Komatsu, E., Dunkley, J., Nolta, M. R., et al. 2009, ApJS, 180, 330
Kravtsov, A. V., Nagai, D., & Vikhlinin, A. A. 2005, ApJ, 625, 588
Kriss, G. A., Cioffi, D. F., & Canizares, C. R. 1983, ApJ, 272, 439
Mendes de Oliveira, C. L., & Carrasco, E. R. 2007, ApJ, 670, L93
Méndez-Abreu, J., Aguerri, J. A. L., Barrena, R., et al. 2012, A&A, 537, A25
Miller, E. D., Rykoff, E. S., Dupke, R. A., et al. 2012, ApJ, 747, 94
Mulchaey, J. S., & Zabludoff, A. I. 1999, ApJ, 514, 133
Navarro, J. F., Frenk, C. S., & White, S. D. M. 1996, ApJ, 462, 563
O'Sullivan, E., Vrtilek, J. M., Kempner, J. C., David, L. P., & Houck, J. C. 2005, MNRAS, 357, 1134
Ponman, T. J., Allan, D. J., Jones, L. R., et al. 1994, Nature, 369, 462
Ponman, T. J., Cannon, D. B., & Navarro, J. F. 1999, Nature, 397, 135
Ponman, T. J., Sanderson, A. J. R., & Finoguenov, A. 2003, MNRAS, 343, 331
Puchwein, E., Sijacki, D., & Springel, V. 2008, ApJ, 687, L53
Rasmussen, J., & Ponman, T. J. 2007, MNRAS, 380, 1554
Santos, W. A., Mendes de Oliveira, C., & Sodré, Jr., L. 2007, AJ, 134, 1551
Sato, S., Akimoto, F., Furuzawa, A., et al. 2000, ApJ, 537, L73
Sato, K., Kawaharada, M., Nakazawa, K., et al. 2010, PASJ, 62, 1445
Sun, M., Forman, W., Vikhlinin, A., et al. 2004, ApJ, 612, 805
Sun, M., Voit, G. M., Donahue, M., et al. 2009, ApJ, 693, 1142
Tozzi, P., Scharf, C., & Norman, C. 2000, ApJ, 542, 106
Vikhlinin, A., Kravtsov, A., Forman, W., et al. 2006, ApJ, 640, 691
Vikhlinin, A., Burenin, R. A., Ebeling, H., et al. 2009, ApJ, 692, 1033
von Benda-Beckmann, A. M., D'Onghia, E., Gottlöber, S., et al. 2008, MNRAS, 386, 2345
Wu, X.-P., Xue, Y.-J., & Fang, L.-Z. 1999, ApJ, 524, 22
Yoshioka, T., Furuzawa, A., Takahashi, S., et al. 2004, Advances in Space Research, 34, 2525
Zibetti, S., Pierini, D., & Pratt, G. W. 2009, MNRAS, 392, 525